United States
Environmental Protection
Agency

Environmental Sciences Research
Laboratory
Research Triangle Park NC 27711

EPA-600/3-79-052
May 1979

Research and Development

Photochemical Aerosol Dynamics

RESEARCH REPORTING SERIES

Research reports of the Office of Research and Development, U.S. Environmental Protection Agency, have been grouped into nine series. These nine broad categories were established to facilitate further development and application of environmental technology. Elimination of traditional grouping was consciously planned to foster technology transfer and a maximum interface in related fields. The nine series are:

1. Environmental Health Effects Research
2. Environmental Protection Technology
3. Ecological Research
4. Environmental Monitoring
5. Socioeconomic Environmental Studies
6. Scientific and Technical Assessment Reports (STAR)
7. Interagency Energy-Environment Research and Development
8. "Special" Reports
9. Miscellaneous Reports

This report has been assigned to the ECOLOGICAL RESEARCH series. This series describes research on the effects of pollution on humans, plant and animal species, and materials. Problems are assessed for their long- and short-term influences. Investigations include formation, transport, and pathway studies to determine the fate of pollutants and their effects. This work provides the technical basis for setting standards to minimize undesirable changes in living organisms in the aquatic, terrestrial, and atmospheric environments.

This document is available to the public through the National Technical Information Service, Springfield, Virginia 22161.

EPA-600/3-79-052
May 1979

PHOTOCHEMICAL AEROSOL DYNAMICS

by

S. K. Friedlander
California Institute of Technology
Pasadena, CA 91125

Grant No. R802160

Project officer

Jack L. Durham
Atmospheric Chemistry and Physics Division
Environmental Sciences Research Laboratory
Research Triangle Park, North Carolina 27711

ENVIRONMENTAL SCIENCES RESEARCH LABORATORY
OFFICE OF RESEARCH AND DEVELOPMENT
U.S. ENVIRONMENTAL PROTECTION AGENCY
RESEARCH TRIANGLE PARK, NORTH CAROLINA 27711

DISCLAIMER

This report has been reviewed by the Environmental Sciences Research Laboratory, U.S. Environmental Protection Agency, and approved for publication. Approval does not signify that the contents necessarily reflect the views and policies of the U.S. Environmental Protection Agency, nor does mention of trade names or commercial products constitute endorsement or recommendation for use.

ABSTRACT

New data are reported on (1) the rate of formation of condensable chemical species by photochemical reactions (2) the effect of the reaction products on the particle size distribution and (3) the distribution of reaction products as a function of particle size.

Gas-to-particle conversion for cyclopentene, cyclohexene and 1,7-octadiene, ranged from 5 to 39 percent of the initial gas-phase carbon concentrations. Size distribution data for cyclohexene were correlated by a diffusion controlled growth law with a Kelvin cutoff diameter at about 0.25 μm.

In polluted atmospheres, some new particle formation takes place as a result of homogeneous gas phase reactions even though an aerosol is already present. To explain the results of laboratory studies of this phenomenon, classical nucleation theory must be modified to take into account the scavenging of clusters by the aerosol.

Using a new low pressure impactor, the first measurements have been made of the distributions of sulfate and nitrate with respect to particle size for $d_p < 0.25$ μm. In Pasadena, the data for sulfate often show a peak in the mass distribution for $0.6 < d_p < 1.0$ μm; less often, a peak is observed near 0.1 μm, consistent with laboratory data for aerosols formed by homogeneous gas phase reactions.

This report was submitted in fulfillment of Grant No. R802160 by the California Institute of Technology, under the sponsorship of the Environmental Protection Agency. This work covers the period April 1, 1973 to March 31, 1978.

CONTENTS

Abstract iii
Figures. vi
Tables. vii

1. Introduction. 1
2. Conclusions 3
3. Nucleation Processes. 4
   Kinetics of homogeneous nucleation 4
   Experimental test of the theory. 5
4. PhotochemicalProcesses. 8
   Photochemically generated condensable species:
      sulfates and nitrates. 8
   Photochemically generated condensable species:
      organics . . . . . .
5. Particle Growth 14
   Heterogeneous condensation 14
   Growth laws. 16
   Measurement of growth laws: organic aerosols 17
6. New particle formation. 22
   Effect of pre-existing aerosol 22
7. Distribution of chemical species with respect to
   particle size. 27
   Distribution of sulfur with respect to particle size . . 27
   Aerosol growth dynamics. 30
   Deviation between theory and experiment: sulfates . . . 31
   Distribution of nitrate with respect to particle size. . 32

References 35

Appendix

A. Project Dissertations and Published Papers. 37

FIGURES

Number		Page
1	The droplet current for supersaturated water vapor at T=300°K calculated from (3)	6
2	Cyclohexene concentration as a function of the integral of the ozone concentration over time	11
3	Number concentrations or particles larger than a given diameter vs diameter at various times in a smog chamber experiment	19
4	Particle growth rates between the fourth and fifth size distribution measurements for the data of Fig. 3	20
5	Aerosol colume distributions for the data of Fig. 3	21
6	Distribution of sulfur with respect to particle size for the ambient aerosol in Pasadena, California, measured with a low pressure impactor	28
7	The distribution of sulfur with respect to particle size for a balloon chamber aerosol, measured with the low pressure impactor	29
8	Aerosol nitrate distributions with respect to particle size for different locations at various times of day	33

TABLES

Number		Page
1	Mechanisms of Gas-to-Particle Conversion.	2
2	Room Temperature Reaction Rate Constants for Hydrocarbons Relevant to Smog Chamber Experiments*	10
3	Fraction of the Initial Hydrocarbon Converted to Aerosol Organic Carbon.	12
4	Aerosol Organic Carbon (AOC) Formation Rates.	13
5	Growth Laws for Gas-to-Particle Conversion.	17

SECTION 1

INTRODUCTION

About 30 percent (annual average) of the aerosol mass in the Los Angeles atmosphere results from gas-to-particle conversion in the atmosphere (Hidy and Friedlander, 1971). The percentage is much greater on days of strong photochemical activity (Grosjean and Friedlander, 1975). This material plays a major role in visibility degradation since it tends to accumulate in the 0.1 to 1.0 μm size range which is most efficient for scattering light. Chemically, it includes sulfate, nitrate and organic compounds, some of which are of public health concern.

Gas-to-particle conversion may result from homogeneous gas phase processes or it may be controlled by processes in the aerosol phase. Gas phase processes, either physical or chemical, can produce a supersaturated state which then collapses by aerosol formation. Physical processes include adiabatic expansion, mixing with cool air, and radiative or conductive cooling.

Gas phase chemical reactions such as the oxidation of SO_2 to sulfuric acid or the reaction of ozone with certain olefins may also generate condensable products. Even if the gas is not saturated with respect to one of the products in its pure form, condensation may take place by the formation or droplets composed of binary solutions.

Once a condensable species has been formed in the gas phase and the system is in a non-equilibrium state, it may pass toward equilibrium either by the generation of new nuclei or by condensation on existing particles. When condensation takes place on existing particles, self-nucleation is suppressed; the existing aerosol scavenges monomer and clusters, and nucleation theory must be modified to predict rates of new particle formation as shown in this report.

Alternatively, molecules from the gas may react on the particle surface or in a droplet. The process can be considered to consist of two steps in series. If the gas-to-particle transport step is rapid compared with the conversion step, the rate of particle growth will be controlled by the rate of chemical conversion in the particulate phase. This is probably the case for SO_2 conversion in droplets in stack plumes when solar radiation is not strong. Table 1 summarizes the various gas-to-particle conversion processes.

Of particular interest in this report are (1) the formation of condensable species by gas-phase photochemical reactions (2) the effect of the condensable products on the particle size distribution and (3) the distribution

of reaction products as a function of particle size. The discussion begins with a brief review of classical nucleation theory; later it is shown how this theory must be modified for photochemically generated pollution aerosols.

TABLE 1. MECHANISMS OF GAS-TO-PARTICLE CONVERSION

I. Homogeneous Nucleation

A. Physical processes producing supersaturation

1. Adiabatic expansion

2. Mixing

3. Conductive cooling

4. Radiative cooling

B. Gas phase chemical reaction

1. Single condensable species (classical theory)

2. Multicomponent condensation (hetermolecular theory)

II. Heterogeneous Condensation

A. Transport limited

1. Diffusion, $d_p >> \ell$

2. Molecular bombardment, $d_p << \ell$

B. Surface controlled chemical reaction or adsorption

C. Particulate phase controlled chemical reaction

SECTION 2

CONCLUSIONS

The secondary aerosol formed in photochemical smog is composed of sulfates, nitrates and organic compounds. Of special interest are the rate of formation of aerosol material, the particle size distribution of the resulting aerosol and the distribution of the different chemical species with respect to particle size.

The results of new laboratory studies of the conversion of four organic gases to aerosol are discussed. The percentage conversion to aerosol depends on two factors--the rate of reaction of the organic aerosol precursor and the physicochemical properties of the reaction products. Cyclopentene is a particularly efficient aerosol precursor; more than a third of the carbon present in the gas phase was converted to aerosol material. The condensable reaction products diffuse to the surfaces of particles in the reacting gas mixture. A critical particle diameter of 0.25 μm below which no growth occurs was observed in experiments with cyclohexene.

A novel experimental study was made of new particle formation in a photochemically reacting gas containing SO_2 with controlled amounts of aerosol present. Classical nucleation theory was not able to explain the experimentally observed rates of new particle formation. A "nucleation barrier"-free model came much closer to predicting observed rates and is justifiable on theoretical grounds. More experimental and theoretical studies of this phenomenon are needed because of its fundamental importance to aerosol dynamics.

Using a specially designed low pressure impactor and a flash-volatilization analysis method, distributions of sulfate and nitrate have been measured for particles as small as 0.05 μm. In laboratory studies with an aerosol present, sulfate tends to accumulate in the size range around 0.1 μm. Ambient measurements in Pasadena usually show a sulfate peak in the 0.6 to 1.0 μm size range but a peak at smaller sizes is sometimes found. More research is needed to explain this discrepancy.

Nitrate distributions were measured at a coastal, an urban and an agricultural site further inland. The coastal nitrate was found in larger particles, probably as a result of droplet phase reaction in the marine aerosol. The measurements made inland showed a nitrate peak in the submicron range. A bimodal nitrate distribution was observed at the urban site located between the other two. The dynamics of nitrate containing aerosols remains poorly understood; both theoretical and experimental studies are needed.

SECTION 3

NUCLEATION PROCESSES

KINETICS OF HOMOGENEOUS NUCLEATION : A REVIEW

The vapor pressure over a small droplet is greater than that over a flat surface of the same liquid (Kelvin effect). This leads in nucleation theory to the existence of a critical droplet diameter, d_p^*, related to the saturation ratio as follows:

$$d_p^* = \frac{4\sigma v_m}{kT\ln S} \tag{1}$$

where σ is the surface tension of the droplet liquid, v_m is the molecular volume, k Boltzmann's constant, and T the absolute temperature. If the saturation ratio, S, is fixed, droplets smaller than d_p^* tend to evaporate while larger ones grow. Calculations based on the observations of Wilson and subsequent measurements by many other experimenters indicate values of d_p^* many times greater than the diameter of a single water molecule, about 2.8 Å. How, then, does condensation take place in systems which have been freed from condensation nuclei by previous expansion or filtration?

Molecular clusters are always present even in an unsaturated gas as a result of collisions among the molecules. When a system becomes supersaturated, these clusers increase in concentration and pass through the critical size d_p^* by attachment of single molecules. The formation of stable nuclei relieves the supersaturation in the gas. Since condensation nuclei are generated by the vapor itself, the process is known as <u>homogeneous nucleation</u> or <u>self-nucleation</u>.

The rate of formation of clusters containing g monomer molecules is called the particle (or droplet) current. It is denoted by the symbol I and has dimensions of particles per cm^3 per second. According to the theory of homogeneous nucleation (Frenkel, 1955) the particle current can be expressed as the sum of two terms:

$$I = -D_v\frac{\partial n}{\partial v} - \frac{D_v}{kT}\frac{\partial \Delta\Phi}{\partial v}n \tag{2}$$

The first term on the right hand side represents the diffusion of particles through particle size (v) space. The coefficient of diffusion is given by the relation

$$D_v = \frac{p_1 \pi d_p^2 v_m}{(2\pi mkT)^{1/2}}$$

where p_1 is the partial pressure of condensing molecules of mass m. D_v has dimensions of (particle volume)^2 sec^{-1}. The second term represents particle transport through v space under the influence of the potential energy.

$$\Delta\Phi = (\Delta\mu)\ g + \pi d_p^2\ \sigma$$

where $\Delta\mu$ is the chemical potential difference between the gas and droplet phases per molecule. As a result of the diffusional term in (2), particles originally present in a given size range will tend to spread over a wider size range as growth occurs.

If the particle current I is independent of cluster size, the following expression can be derived (Frenkel, 1955):

$$I = 2\left[\frac{p_1}{(2\pi mkT)^{1/2}}\right]\left(n_1 v_m^{2/3}\right)\left[\frac{\sigma v_m^{2/3}}{kT}\right]^{1/2} \exp - \frac{16\pi\sigma^3 v_m^2}{3(kT)^3(TnS)^2} \qquad (3)$$

The first term in brackets is the monomer flux (molecules per unit area per unit time) and the second is proportional to the monomer surface area per unit volume of gas. Their product has the same dimensions as I, number per unit volume per unit time. The group $\sigma v_m^{2/3}/kT$ is dimensionless. The last term includes an exponential factor, the "nucleation barrier," a term much less than unity when the saturation ratio is small (nearly unity).

The droplet current calculated from (3) is shown in Figure 1 for water vapor at a temperature of 300°K. Order of magnitude increases in I result from small increases in S, primarily because of the dependence on ln S in the argument of the exponential function. Although a supersaturated vapor is always unstable, the rate of generation of stable nuclei is negligible for small values of S. When I = 1 drop/cm^3 sec, particle formation can be conveniently observed experimentally. The corresponding value of S is designated the critical saturation ratio, S_{crit}.

EXPERIMENTAL TEST OF THE THEORY

It is difficult to carry out experimental studies capable of verifying the theory. Measurements of the nuclei size spectrum would constitute a sensitive check, but instruments capable of measurement in the 10 to 100 Å size range have not been available. Most experimental tests have involved measurements of the saturation ratio at which condensation occurs using an expansion (Wilson) cloud chamber. Data collected with the chamber are difficult to interpret because of the unsteady nature of the expansion process. These investigations are reviewed by Mason (1971).

The diffusion cloud chamber is a particularly attractive experimental system for the study of nucleation kinetics; it is compact and produces a well-defined, steady supersaturation field. The chamber is cylindrical in

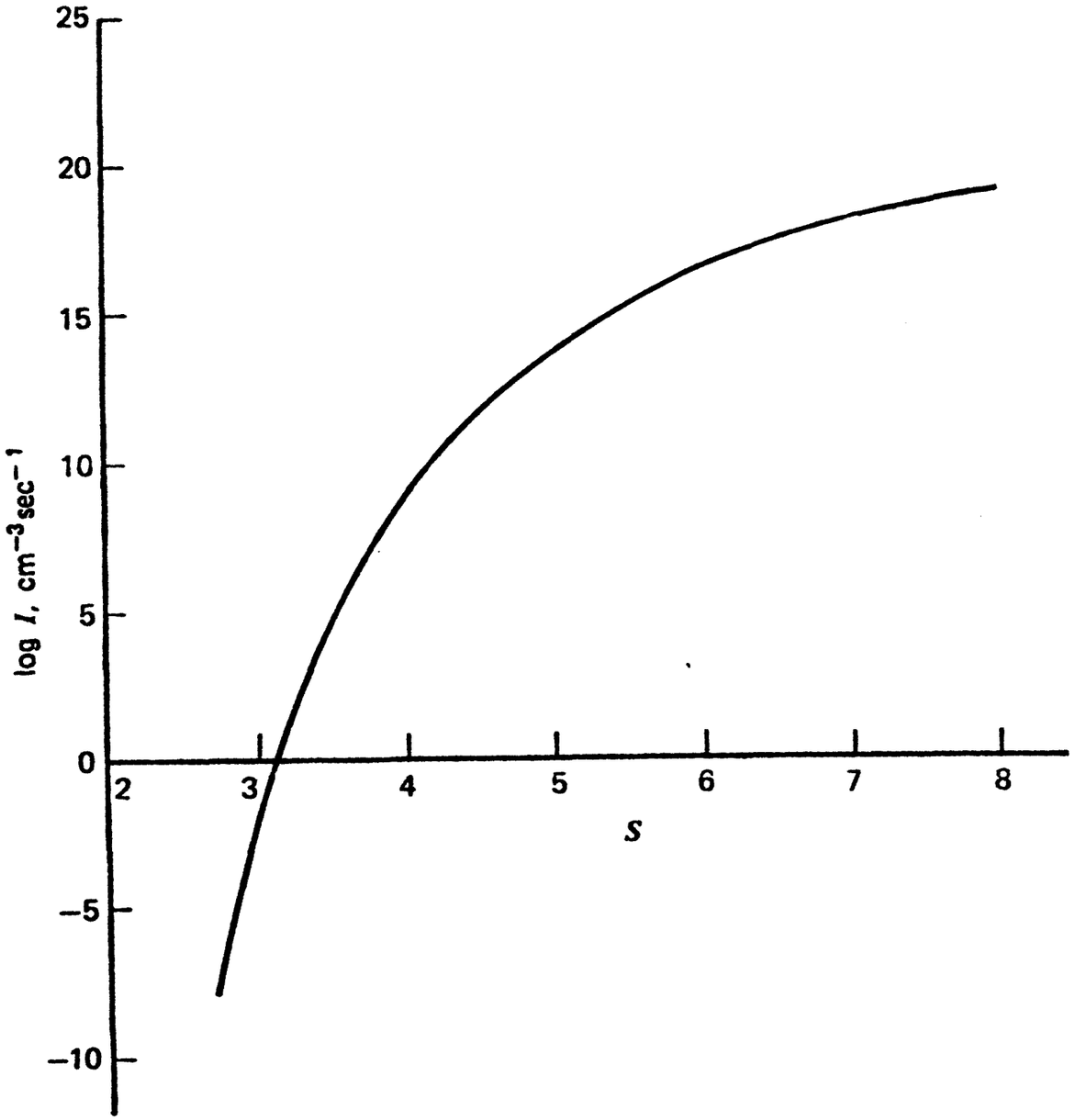

Figure 1. The droplet current for supersaturated water vapor at T = 300°K calculated from (3). The critical saturation ratio, corresponding to I = 1 cm^{-3} sec, is about 3.1.

shape, perhaps 30 cm in diameter and 4 cm high. A heated pool of liquid at the bottom of the chamber evaporates into a stationary carrier gas, usually hydrogen or helium. The vapor diffuses to the top of the chamber, which is cooled, condenses and drains back into the pool at the bottom. Since the vapor is denser than the carrier gas, the density is greatest at the bottom of the chamber and the system is stable with respect to convection. Both diffusion and heat transfer are one dimensional, with transport occurring from the bottom to the top of the chamber. At some position in the chamber, the temperature and vapor concentrations reach levels corresponding to supersaturation. The variation in the properties of the system are calculated by numerical integration of the one dimensional equations for heat conduction and mass diffusion. The saturation ratio is calculated from the computed local partial pressure and vapor pressure.

The goal of an experiment is to set up a "critical" chamber state, that is, a state which just produces nucleation at some height in the chamber where the vapor is critically supersaturated and droplets are visible. This occurs when the temperature difference across the chamber has been increased to the point where a rain of drops forms at an approximately constant height. Observed and predicted saturation ratios can then be compared.

Good agreement between theory and experiment has been obtained with this system for a variety of organic compounds (Katz et al., 1975). For water, agreement is poorer (Heist and Reiss, 1973). Such experiments offer the most convincing support yet developed for the theory of homogeneous nucleation.

This brief review of theory and experiment for homogeneous nucleation has set the stage for the more complex processes leading to aerosol formation in polluted atmospheres.

SECTION 4

PHOTOCHEMICAL PROCESSES

PHOTOCHEMICALLY GENERATED CONDENSABLE SPECIES: SULFATES AND NITRATES

In the experiments discussed in the last section, the supersaturated state was produced by a set of physical processes. Gas phase chemical reactions may also lead to the formation of condensable species and several may be present simultaneously. Of special air pollution interest are reactions involving SO_2, NO-NO_2 and certain organic compounds.

The rate of SO_2 conversion to particulate sulfur (usually $(NH_4)_2SO_4$) in the Los Angeles atmosphere, heavily polluted by the organic vapors and nitrogen oxides in automobile exhaust, ranged from 1-13% per hour in measurements reported by Roberts and Friedlander (1975). The SO_2 is probably oxidized by certain free radicals present in photochemical smog. The most important such radicals are thought to be the hydroxyl, OH:

$$SO_2 + OH + M \rightarrow HSO_3 + M$$

the hydroperoxyl, HO_2:

$$SO_2 + HO_2 \rightarrow SO_3 + OH$$

and peroxyalkyl, RO_2:

$$SO_2 + RO_2 \rightarrow SO_3 + RO$$

where R represents an alkyl group. The conversion of HSO_3 formed in the first reaction, to H_2SO_4 is believed to occur rapidly but the mechanism has not been established. Rate constants for reactions of the last type are not well known and more data are needed to assess their importance for the atmospheric oxidation of SO_2. Calculations based on the kinetics of known reactions involving SO_2 have not been able to account for SO_2 oxidation rates measured in smog chamber studies (Sander and Seinfeld, 1976).

Particulate nitrates may be formed in the atmosphere by the gas-phase oxidation of NO to NO_2 and then to nitric acid. Nitrogen oxides are produced in combustion processes and emitted into the atmosphere in large quantities by power plants and automobiles. Calvert (1973) considers oxidation by the hydroxyl radical the principal mode of formation

$$HO + NO_2 + M \rightarrow HONO_2 + M$$

where M represents a third body. The aerosol nitrate is usually present as the ammonium salt in polluted atmospheres. This form may result from gas phase reaction of nitric acid with ammonia or from reaction in the droplet phase.

If only a single condensable species is formed by chemical reaction, it may condense by homogeneous nucleation in the absence of existing particles. In other cases, two or more condensable species may be present simultaneously in the gas. If these form solution droplets, nucleation can take place at partial pressures much lower than those required for nucleation of pure vapors. The theory of this type of homogenous nucleation, known at heteromolecular nucleation, is a modified version of the theory for a single component discussed in an earlier section (Reiss, 1950). An application of the theory to the sulfuric acid-water and nitric acid-water systems has been made by Kiang and Stauffer (1973) and Mirabel and Katz (1974).

PHOTOCHEMICALLY GENERATED CONDENSABLE SPECIES: ORGANICS

Certain diolefins and cyclic olefins are very efficient aerosol precursors. Grosjean and Friedlander (1978) studied the formation of organic aerosols using mixtures of NO, NO_2 (0.15 to 0.30 ppm) and olefins (0.5 to 2.0 ppm). These were added to atmospheric air (Pasadena) and allowed to react in sunlight for up to three hours in a large outdoor chamber constructed from 2 mil FEP Teflon film located on the roof of the Keck Laboratories at Caltech. The chamber surface was about 117 m^2 and the initial chamber volume ranged from 53 to 134 m^3. Four olefins were studied: 2,3-dimethyl-2 butene, cyclopentene, cyclohexene, and 1,7 octadiene.

Olefin concentration as a function of time was measured during several of the cyclopentene, cyclohexene and 1,7-octadiene runs. Ozone appearance in these systems always coincided with a marked increase in hydrocarbon consumption.

The rate of olefin reaction can be written as a sum of biomolecular reaction rate terms:

$$- d[HC]/dt = \sum_i k_i [X_i] [HC] \qquad (4)$$

where k_i are the second order rate constants of hydrocarbon attack by the species X_i, with X_i = 0, OH, O_3 HO_2, etc. Assuming that only one species reacts with the olefin:

$$- d[HC]/dt = k_i [X_i] [HC]$$

$$\text{or:} \quad \log [HC] = \log [HC]_o + \frac{k_i}{2.303} \int_o^t [X_i] \, dt$$

where $[HC]_o$ is the initial hydrocarbon concentration.

Therefore, the relative importance of ozone in the overall hydrocarbon consumption can be tested further by plotting log [HC] as a function of $\int_0^t [O_3]dt$, as is shown in Figure 2 for cyclohexene. With the exception of the first ∿ 10 minutes during which an "excess rate" was observed, a good linear relationship was observed throughout the experiment, with a slope corresponding to a cyclohexene-ozone rate constant of 0.15 ppm^{-1} min^{-1}. The reactivity of the four hydrocarbons (2,3-dimethyl-2 butene > cyclopentene > cyclohexene > 1,7-octadiene) was consistent with their known rates of reaction with ozone and with the hydroxyl radical OH (Table 2). It was difficult, however, to assess the relative importance of the two species in these experiments.

TABLE 2. ROOM TEMPERATURE REACTION RATE CONSTANTS FOR HYDROCARBONS RELEVANT TO SMOG CHAMBER EXPERIMENTS* (GROSJEAN & FRIEDLANDER 1978)

Hydrocarbon	O_3(a)	OH(b)	$O(^3P)$(c)	NO(d)
2,3-dimethyl 2-butene	1510	110	5.11	59
cyclopentene	813	No data (ND)	1.79	23
cyclohexene	169	62.4	1.62	3.5
1,7-octadiene	ND	ND	ND	ND
1-hexene (g)	8.4	31.2	0.39	1.7
1,3-butadiene (g)	11.1	68.5	1.45	4.3

* Original references given by Grosjean and Friedlander, 1978.

a) k_{O_3} in 10^{-18} cm^3 $molecule^{-1}$ sec^{-1}.

b) k_{OH} in 10^{-12} cm^3 $molecule^{-1}$ sec^{-1}.

c) k_O in 10^{-11} cm^3 $molecule^{-1}$ sec^{-1}.

d) Nitric oxide photooxidation rate, ppb^{-1} min^{-1}.

Aerosol samples were analyzed for their organic carbon content, which averaged only ∿ 35 percent by weight of the total aerosol. Inorganic nitrate was also produced in all runs and accounted for ∿ 10 percent by weight of the aerosol. Thus, the low carbon fraction indicates that the aerosol products formed are highly oxygenated species averaging ∿ 40-45 percent carbon by weight. This is indeed the case for the major organic products identified in these runs, for example adipic acid and 6-nitrato hexanoic acid (carbon = 41 percent) from cyclohexene.

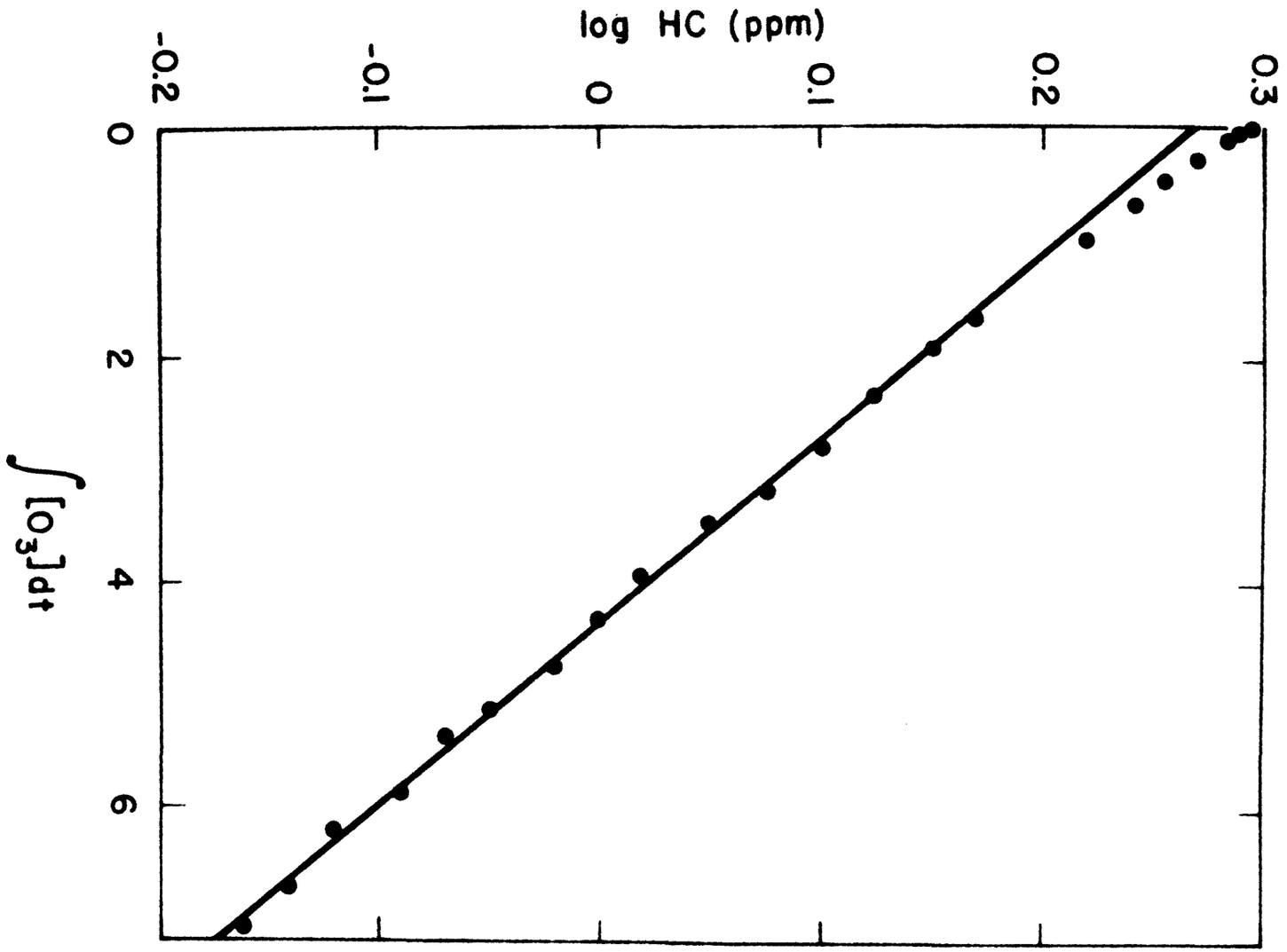

Figure 2. Cyclohexene concentration as a function of the integral of the ozone concentration over time. The straight line is observed consistent with a bimolecular reaction between cyclohexene and ozone (and species accompanying ozone).

Final aerosol organic carbon concentrations ranged from 5 to 39 percent of the initial hydrocarbon concentrations (Table 3) for cyclopentene, cyclohexene and 1,7-octadiene. Thus, most of the products resulting from photooxidation of the olefinic hydrocarbons studied remain in the gas phase. On the other hand, cyclopentene, cyclohexene and 1,7-octadiene are more potent organic aerosol precursors than the hydrocarbon mix present in ambient Southern California air where carbon-gas-particle distribution factors of only 1 to 3 percent are measured (Grosjean and Friedlander, 1975).

Aerosol organic carbon formation rates are listed in Table 4 and ranged from 1.5 to 41 μg carbon m^{-3} min^{-1}. In all runs these rates paralleled the rate of formation of ozone and the product of the hydrocarbon and ozone concentrations, i.e., increased to the maximum values listed in Table 4 and then decreased upon further irradiation. Thus, aerosol formation rates were found to correlate in an approximately linear fashion with the product of the olefin and ozone concentrations. An empirical relation of the general form: $d(\text{aerosol})/dt = \alpha[O_3]\,[HC]$ does not necessarily imply that organic aerosol is produced only as a result of the ozone-olefin reaction. The relation may be composite, i.e, may include terms representing the contribution of other species including the hydroxyl radical.

Assuming this relation holds for urban atmospheres (not necessarily a good assumption) one obtains, for typical ozone (0.1 ppm) and hydrocarbon (10 ppb) concentrations, organic aerosol production rates of ∿ 0.02, 0.15, and 0.6 μg carbon m^{-3} min^{-1} for 1,7-octadiene, cyclohexene and cyclopentene,

TABLE 3. FRACTION OF THE INITIAL HYDROCARBON CONVERTED TO AEROSOL ORGANIC CARBON (GROSJEAN, 1978)

Hydrocarbon	Run No.	A/B(a)(b)	Hydrocarbon	Run NO.	
Cyclohexene	A07	0.10	2,3-dimethyl-2-butene	E01	0.0
	A91	0.06			
	A08	0.5	1,7-octadiene	F04	---
	A09	0.06		F05	0.11
	A92	0.07		F91	0.13
	A10	0.06		F06	0.07
	A11	0.14			
	A12	0.17	Cyclopentene	F01	0.33

a) A = aerosol organic carbon measured at the end of the run, $\mu gm^{-3}C$; G = initial hydrocarbon concentration, converted from ppm to μg $m^{-3}C$ (A/G is a dimensionless number).

b) A/G are presumably upper limits since some artifact aerosol is expected to form during sampling by adsorption of volatile acidic organics on the surface of the basic glass fiber filters.

respectively. For comparison purposes, average rates of aerosol organic carbon production in Southern California on smoggy days are of the order of 0.5 μg carbon m^{-3} min^{-1} (estimated from the measured particulate organic carbon levels in the eastern part of the Los Angeles Basin, 30 μg carbon m^{-3} and assuming an air parcel transport time of 10 hours.

TABLE 4. AEROSOL ORGANIC CARBON (AOC) FORMATION RATES

Hydrocarbon	Run No.	d(AOC)/dt, μg C m^{-3} min^{-1} average	maximum
Cyclohexene	A12	16	39
Cyclopentene	G01	41	78
	G03	9.1	33
1,7-octadiene	F05	2.5	3.2
	F91	4.3	8.0
	F06	1.5	2.5

SECTION 5

PARTICLE GROWTH

HETEROGENEOUS CONDENSATION

When large concentrations of particles are present and the saturation ratio is low, condensation takes place on the existing particles without formation of new nuclei. We call this process heterogeneous condensation. Cloud formation in the atmosphere takes place in this way since supersaturations are usually less than a few percent and nuclei concentrations are high.

The rate of heterogeneous condensation depends on the exchange of matter and heat between a particle and the continuous phase. The extreme cases of a particle much larger or much smaller than the mean free path of the suspending gas, ℓ, are easy to analyze. In the continuum range, ($d_p >> \ell$) diffusion theory can be used to calculate the transport rate. For a single sphere in an infinite medium, the steady state equation of diffusion in spherical coordinates takes the form

$$\frac{\partial n}{\partial t} = \frac{D\partial r^2 \frac{\partial n}{\partial r}}{r^2 \partial r} = 0 \tag{5}$$

where n is the molecular concentration of the condensing species and D is its coefficient of diffusion. The solution which satisfies the boundary conditions $n = n_d$, the concentration in equilibrium with the surface at $r = d_p/2$ and $n = n_1$ at $r = \infty$ is

$$\frac{n - n_d}{n_1 - n_d} = \frac{d_p}{2r} \tag{6}$$

The rate of diffusional condensation is given by

$$F = D\left(\frac{\partial n}{\partial r}\right)_{r=d_p/2} \pi d_p^2 = 2 \pi d_p D(n_1 - n_d) \tag{7}$$

$$= 2 \mu d_p D(p_1 - p_d)/kT$$

where F is the flow of molecules (number per unit time) to the surface of

the particle. The surface concentration, n_d, is determined by the surface temperature and curvature. It is assumed that the condensation rate is sufficiently slow for the latent heat of condensation to be dissipated without changing droplet temperature.

For particles much smaller than the mean free path of the gas the rate of condensation can be calculated from kinetic theory. The net molecular flux at a surface of area πd_p^2 is given by:

$$F = \frac{\alpha(p_1 - p_d)\pi d_p^2}{(2\pi mkT)^{1/2}} \tag{8}$$

At one atmosphere, this expression applies to particles smaller than about 0.06 μm. Separate accommodation coefficients, α, are often introduced for the condensation, $p_1/(2\pi mkT)^{1/2}$ and evaporation, $p_d/(2\pi mkT)^{1/2}$, fluxes but the values are assumed equal in (8). In general, these coefficients must be determined experimentally. An approximate interpolation formula for the entire range of mean free path has been proposed by Fuchs and Sutugin (1971):

$$F = 2\pi D d_p (n_1 - n_d) \left\{ \frac{1 + Kn}{1 + 1.71Kn + 1.333Kn^2} \right\} \tag{9}$$

where the Knudsen number $Kn = 2\ell/d_p$ and ℓ is the mean free path for collision of the condensing species. When $Kn << 1$, (9) reduces to (7) for the continuum range. When $Kn >> 1$, (9) is about 1.2 times (8) with $\alpha = 1$ for rigid elastic spheres.

When the Kelvin effect is important, the partial pressure driving force for condensation takes the form

$$\begin{aligned}(p_1 - p_d) &= p_1 - p_s \exp\left[\frac{4\sigma v_m}{d_p KT}\right] \\ &= p_1 - p_s \exp\left[\frac{d_p^* \ell nS}{d_p}\right]\end{aligned} \tag{10}$$

where p_s is the vapor pressure over a flat surface or pool of liquid and d_p^* is the critical droplet diameter. It has been assumed that the nucleus behaves like a pure drop of the condensing species. If the surface of the particle is composed of a material different from that of the condensing vapor, this result must be modified to account for surface wetting effects.

Expanding the exponential of (10)

$$\Delta p = p_s [S - 1 - \frac{d_p^*}{d_p} \ell nS - \frac{1}{2} \left(\frac{d_p^*}{d_p} \ell nS\right)^2 - \ldots$$

where $S = p_1/p_s$. For small values of S-1, this takes the approximate form

$$\Delta p = \frac{p_s}{d_p} (S-1) (d_p - d_p^*) \tag{11}$$

As an example, this result can be substituted in (7) for growth by diffusion in the continuum range:

$$F = \left(\frac{2\pi D}{KT}\right) p_s (S-1)(d_p - d_p^*) \qquad (S-1 \ll 1) \tag{12}$$

The rate of condensation is proportional to the difference between the particle diameter and the critical particle diameter.

GROWTH LAWS

Growth laws are expressions for dv/dt or $d(d_p)/dt$ as functions of particle size and the appropriate chemical and physical properties of the system. Such expressions are necessary for the calculation of changes in the size distribution function with time as shown in the next section. When growth is transport limited, the rate can be determined from the expressions derived in the previous section. For the continuum range, the growth law based on (7) is given by:

$$\frac{dv}{dt} = \frac{2\pi D d_p v_m}{KT} (p_1 - p_d)$$

The effect of the moving boundary of the growing particle is neglected.

For nuclei smaller than the mean free path of the gas, the growth law, based on (8) is given by:

$$\frac{dv}{dt} = \frac{\pi d_p^2 v_m (p_1 - p_d)}{(2\pi mKT)^{1/2}}$$

where the accommodation coefficient α has been set equal to unity.

Chemical reactions at particle surfaces are likely to be most important near aerosol sources where the particle surfaces are fresh and their catalytic activity high. (In the atmosphere, however, contamination probably destroys the specific catalytic activity of aerosol surfaces.) Particles will grow if the products of reaction accumulate at the surface. When reaction rates are fast compared with transport, growth laws are of the same form as the transport limited laws. When reaction rates are slow compared with transport, the concentration of the reactive species in the gas near the surface is practically the same as in the bulk of the gas, and the rate of conversion is determined by the fraction of the collisions with the surface which are effective:

$$\frac{dv}{dt} = \frac{\alpha P_1 \pi d_p^2 v_m}{(2\pi mKT)^{1/2}}$$

where α, the fraction of effective collisions, is usually much less than unity.

Examples of growth laws including those limited by chemical reaction in the particulate phase are summarized in Table 5. The dependence of dv/dt varies from d_p for diffusion in the continuum range to d_p^3 for droplet phase chemical reaction. Different forms for the growth law can lead to significantly different changes in the size distribution function with time and to the distribution of chemical species with respect to size.

TABLE 5. GROWTH LAWS FOR GAS-TO-PARTICLE CONVERSION

Mechanism	Growth Law, dv / dt
Diffusion ($d_p >> 1$)	$\frac{2\pi D d_p v_m (P_1 - P_d)}{KT}$
Molecular bombardment ($d_p << 1$)	$\frac{\alpha \pi d_p^2 v_m (P_1 - P_d)}{(2\pi mKT)^{1/2}}$
Surface reaction (all sizes)	$\frac{\alpha \pi d_p^2 v_m P_1}{(2\pi mKT)^{1/2}}$ $(\alpha << 1)$
Droplet phase reaction	$\frac{\pi d_p^3}{6\rho_p} (\sum M_i v_i) r$

(Friedlander, 1977)

MEASUREMENT OF GROWTH LAWS: ORGANIC AEROSOLS

The growth law for a polydisperse aerosol can be determined by measuring the change in the size distribution function with time. In experiments carried out by Heisler and Friedlander (1977), small amounts of certain organic vapors, which served as aerosol precursors, were added to a sample

of the normal atmospheric aerosol contained in an 80 m^3 bag exposed to solar radiation. Small concentrations of nitrogen oxides were also added. The bag was made of Teflon which is almost transparent to solar radiation in the uv range and relatively unreactive chemically. Photochemical reactions involving the nitrogen oxides lead to the formation of ozone and hydroxyl radicals which reacted with the organic vapors to produce condensable species as discussed in a previous Section. The change with time of the size distribution function was measured with a single particle optical counter.

The number of particles per unit volume larger than a given particle size d_p, $\int_{d_p}^{\infty} n_1(\tilde{d}_p)d(\tilde{d}_p)$, is shown in Figure 3 for an experiment with cyclohexene. Consider a horizontal line on the figure corresponding to constant values of this integral. In the absence of homogeneous nucleation, each such line corresponds to the growth with time of a particle of size given initially by the curve for t=0. No particle can move across such a line because the total number larger is conserved.

The growth rate, $d(d_p)/dt \approx \Delta d_p/\Delta t$ can be obtained from adjacent distributions in Figure 3 as a function of d_p and of time. The data were then plotted with dv/dt as a function of particle diameter as shown in Figure 4. For this set of data, an approximately linear relationship was found with an intercept on the positive d_p axis.

As a reasonable model for explaining these results, it was assumed that a single condensable species was formed in the gas as a result of chemical reaction, or a small group of species with similar thermodynamic properties. Molecules of these reaction products then diffused to the surfaces of existing aerosol particles. Hence a diffusion controlled growth law modified by the Kelvin effect in the small saturation ratio approximation (11) correlated the data as shown in Figure 4. The cutoff particle diameter probably resulted from the Kelvin effect. For the run shown, the critical diameter was about 0.28 μm. The line is the result of a least-squares fit using (9) combined with (11) in calculating the growth law. The curvature in the line results from the form of the interpolation formula (9).

Aerosol volume distributions calculated from the data are shown in Figure 5. Material accumulates in the size range near 0.6 μm which is particularly efficient for light scattering. Small particles grow little because of the Kelvin effect.

In experiments with cyclopentene, the data showed a pronounced bend at a particle diameter larger than the lower cutoff diameter. The results were correlated by Heisler and Friedlander (1976) using a growth law which incorporated another condensing species.

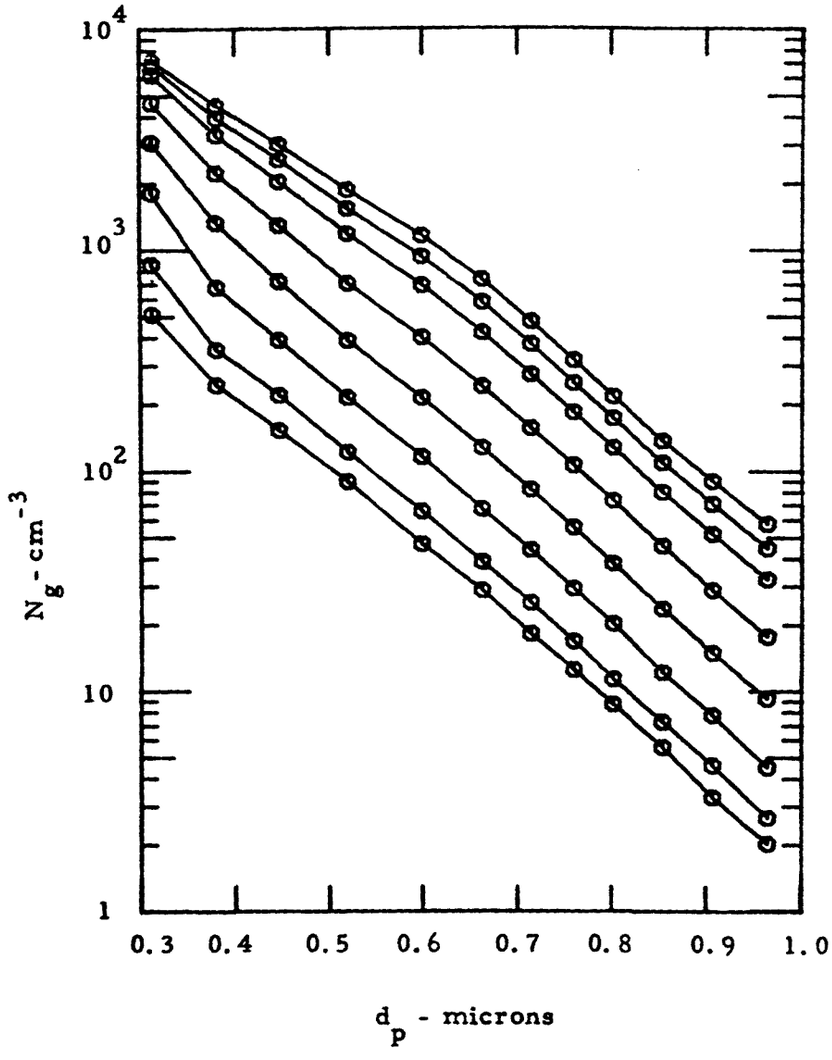

Figure 3. Number concentrations or particles larger than a given diameter vs diameter at various times in a smog chamber experiment. Initial concentrations were 2.02 ppm cyclohexene, 0.34 ppm NO and 0.17 ppm NO_2. The time between measurements shown was made 12 minutes after the addition of the reactants (Heisler and Friedlander, 1977).

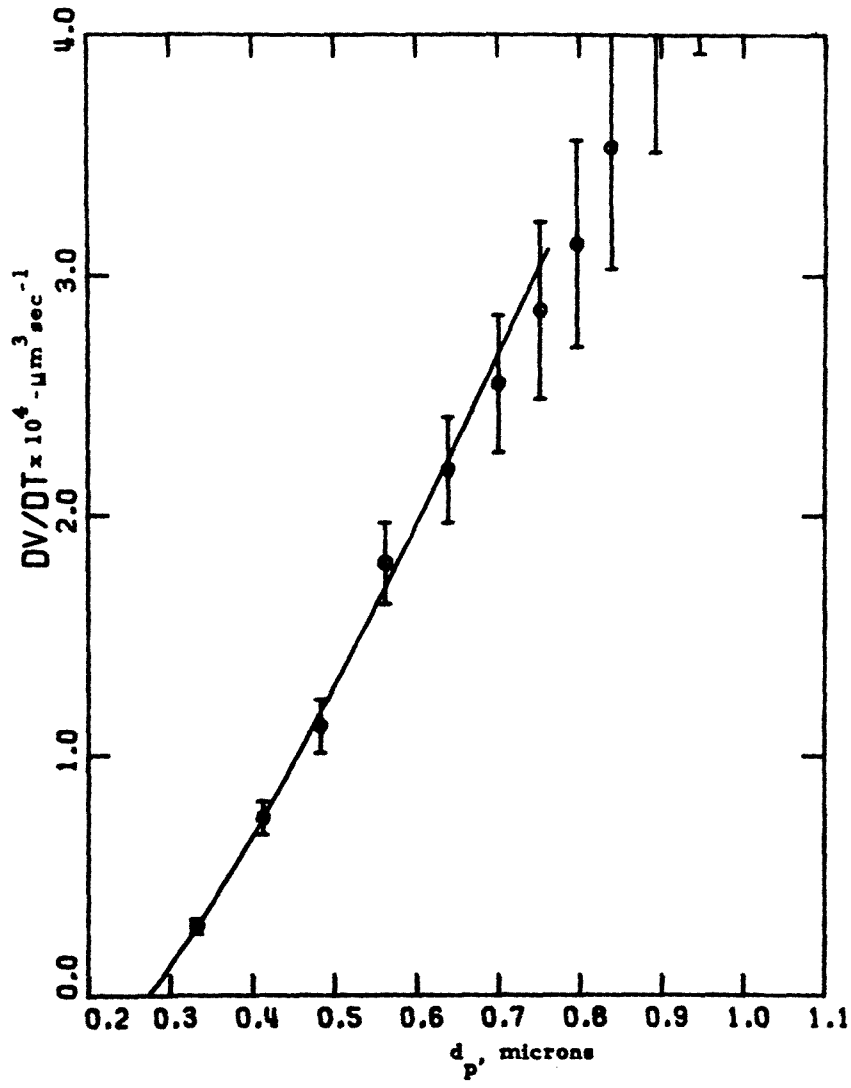

Figure 4. Particle growth rates between the fourth and fifth size distribution measurements for the data of Fig. 3. The solid line is a least-square fit of the diffusional growth law, modified to include mean free path effects and the Kelvin effect. The intercept on the size axis is the average critical size, d_p^* (Heisler and Friedlander, 1977).

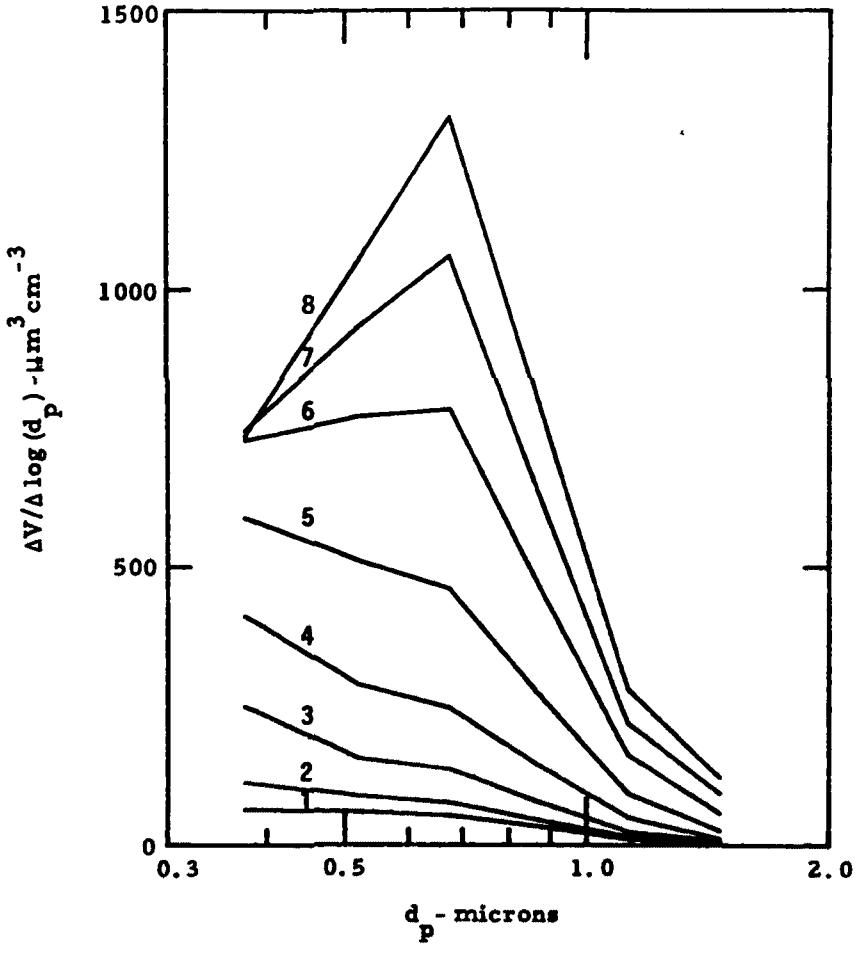

Figure 5. Aerosol volume distributions for the data of Fig. 3. The order of the measurements is indicated by the numbers. Increases are from gas-to-particle conversion. The peak is near the size range most efficient for light scattering (Heisler and Friedlander, 1977).

SECTION 6

NEW PARTICLE FORMATION

EFFECT OF PRE-EXISTING AEROSOL

There is good evidence that in polluted atmospheres some new particle formation takes place even though an aerosol is already present (McMurry, 1977). In this section, the effect of the aerosol on the rate of new particle formation is examined. The aerosol will, of course, collect monomer molecules of the condensable species generated by chemical reaction; in the past, it has usually been assumed that rates of nucleation can be calculated from Equation (3) derived for particle-free gases. However, as shown in this section, the classical theory must be modified because of the scavenging of clusters by the aerosol.

We consider first the case of particle formation in the absence of an aerosol. Let n_g be the concentration of clusters containing g monomer molecules. The time rate of change in n_g as a result of particle growth processes is given by (Frenkel, 1955; Friedlander, 1977):

$$\frac{\partial n_g}{\partial t} = I_g - I_{g+1} \tag{13}$$

where I_g, the particle (droplet) current is the net rate of formation of particles of size g from clusters of size g-1. The net rate of loss of particles of size g to the range g+1 by growth processes is I_{g+1}. Collision and coagulation among the clusters is neglected. In classical nucleation theory, a steady state is assumed and $\frac{\partial n_g}{\partial t} = 0$. Thus $I_g = I_{g+1}$ = constant = I. The result of a theoretical analysis gives Equation (3) for I.

If an aerosol composed of larger particles ($d_p > 0.05$ μm, say) is already present, (13) must be modified. Clusters deposit on the pre-existing aerosol at a rate proportional to the aerosol surface area if the particles are smaller than the mean free path of the carrier gas. (It is assumed that the aerosol particles are uniformly dispersed on a scale comparable to that on which the chemical reactions are taking place). This introduces a new term into the continuity relation, (13):

$$\frac{\partial n_g}{\partial t} = I_g - I_{g+1} - n_g\left(\frac{kT}{2\pi m_g}\right)^{1/2} A \tag{14}$$

where k = Boltzmann's constant

T = absolute temperature

m_g = mass of cluster of size g

A = surface area of pre-existing aerosol per unit volume of gas

Making the steady state assumption, this equation becomes

$$I_g - I_{g+1} = n_g \left(\frac{KT}{2\pi m_g}\right)^{1/2} A \tag{15}$$

Changes in A with time resulting from gas-to-particle conversion are assumed to be small. As a result of cluster deposition on the surface area A, the particle current I_g is no longer independent of size but decreases with increasing cluster size.

The particle current can be written as follows Frenkel (1955):

$$I_g = \beta n_{g-1} s_{g-1} - \alpha_g n_g s_g \tag{16}$$

where β the monomer flux is given by

$$\beta = n_1 \left(\frac{KT}{2\pi m_1}\right)^{1/2}$$

and α_g the evaporative flux is given by

$$\alpha_g = \beta \frac{s_{g-1}}{s_g} \exp\left[\frac{4\sigma v_1}{d_p KT} - \ln S\right] \tag{17}$$

Also s_g = surface area of a cluster

σ = surface tension

v_1 = volume of monomer molecule

d_p = cluster diameter

S = saturation ratio

In the special case of negligible evaporative flux, (16) becomes

$$I_g = \beta n_{g-1} s_{g-1}$$

Substitution in the steady state expression gives:

$$n_{g-1}s_{g-1} - n_g s_g = \frac{n_g A}{g^{1/2} n_1}$$

Rearranging

$$\frac{n_{g-1}s_{g-1}}{n_g s_g} = 1 + \frac{A}{g^{1/2} s_g n_1} \tag{18}$$

If the surface area of the foreign aerosol is large, $A/g^{1/2}s_g n_1 >> 1$ and this expression becomes

$$\frac{n_{g-1}s_{g-1}}{n_g s_g} \simeq \frac{A}{g^{1/2} s_g n_1}$$

The cluster size distribution is given by

$$\frac{n_1 s_1}{n_2 s_2} \cdot \cdot \cdot \frac{n_{g-1}s_{g-1}}{n_g s_g} = \frac{n_1 s_1}{n_g s_g} = \frac{A}{s_2 n_1} \cdot \cdot \cdot \frac{A}{g^{1/2} s_g n_1} \tag{19a}$$

or

$$\frac{n_g s_g}{n_1 s_1} = \frac{[g!]^{7/6}}{[A/n_1 s_1]^{g-1}} \qquad \left[\frac{A}{s_1 n_1 g^{7/6}} >> 1\right] \tag{19b}$$

The rate of new particle formation is given by

$$I_{g+1} = \beta n_g s_g = \frac{\beta n_1 s_1 [g!]^{7/6}}{[A/n_1 s_1]^{g-1}} \tag{20}$$

with the same constraint given in (19b).

It is not necessary for the evaporative flux to vanish for this analysis to hold at least approximately. Inspection of (16) indicates that the second (evaporative) term will be much smaller than the first provided that

$$n_g s_g \; g \ll n_{g-1} s_{g-1} \beta$$

or

$$\frac{n_{g-1} s_{g-1}}{n_g s_g} \gg \frac{\alpha g}{\beta} = \frac{n^*_{g-1} s_{g-1}}{n^*_g s_g}$$

where the asterisk refers to the equilibrium distribution. This means that the evaporative flux can be neglected provided that the cluster size distribution is much steeper than the equilibrium distribution.

The largest value of α_g/β occurs for a cluster of size $g = 2$. The value of this ratio for the critical cluster size is unity; for larger particles, the value falls below one, approaching S^{-1} as $g \to \infty$.

The ratio α_g/β can also be expressed as follows using (17)

$$\frac{\alpha_g}{\beta} = \frac{s_{g-1}}{s_g} \exp\left[\left(\frac{d^*_p}{d_p} - 1\right) \ln S\right] \tag{21a}$$

$$= \frac{s_{g-1}}{s_g} S^{[(d^*_p/d_p)-1]} \tag{21b}$$

$$= \left(\frac{g-1}{g}\right)^{2/3} S^{[(g^*/g)^{1/3}-1]} \tag{21c}$$

where the critical particle diameter is given by

$$d^*_p = \frac{4\sigma v_1}{KT \ln S}$$

For the case of the dimer, the values of α_2/β can be calculated from (21c) with the following values assumed:

$$S = 10$$

$$g^* = 8$$

then

$$\frac{\alpha 2}{\beta} = \left(\frac{1}{2}\right)^{2/3} 10^{0.59} = 2.45$$

This is to be compared with the ratio of (18):

$$\frac{n_{g-1}s_{g-1}}{n_g s_g} = 1 + \frac{A}{s_1 n_1 g^{7/6}}$$

As reasonable values for the Los Angeles smog aerosol, we take $A = 2 \times 10^{-5}$ cm^{-1} and $n_1 = 10^8$ cm^{-3}, and a molecular diameter = 5×10^{-8} cm.

Then

$$1 + \frac{A}{s_1 n_1 g^{7/6}} = 1 + \frac{2(10)^{-5}}{\pi(5 \times 10^{-8})^2 (10)^8 2^{7/6}}$$

$$= 12.34$$

For this set of assumed values, the evaporative term will be small compared with the condensation term.

These calculations indicate that when the surface area of the pre-existing aerosol is large and the rate of formation of condensable species is low, clusters are scavenged by the aerosol at a rapid rate. The slope of the steady-state cluster distribution with respect to particle size is much steeper than the slope of the equilibrium distribution. As a result, the evaporative term in the expression for the particle current can be neglected and a term for the "nucleation barrier" does not appear in the expression for the particle current, (20). The rate of new particle formation is controlled by the pre-existing aerosol. The particle current is much smaller than in the absence of foreign particles; most of the condensable species deposits on the aerosol and little condensing mass grows through the 10 to 100 Å size range to appear as new particles.

McMurry (1977) has studied the effect of an aerosol on the rate of new particle formation in the SO_2-NO_x-propylene system. Experiments were performed in a teflon balloon reaction exposed to solar radiation. The concentration of the rate of formation of particles larger than 100 Å with electrical aerosol analyzer. He found approximate agreement between his experimental results and a nucleation barrier-free theoretical calculation, as expected from the above considerations.

SECTION 7

DISTRIBUTION OF CHEMICAL SPECIES WITH RESPECT TO PARTICLE SIZE

DISTRIBUTION OF SULFUR WITH RESPECT TO PARTICLE SIZE

The development of a low pressure impactor capable of fractionating aerosol particles larger than about 200 Å has been described by Hering, Flagan and Friedlander (1977). The impactor has eight single jet stages corresponding to a particle collected with an efficiency of 50% are 4.0, 2.0, 1.0, 0.5, 0.26, 0.11, 0.076, and 0.05 μm. The cutoff diameter for the last two stages are approximate, based in part on calculation and in part on an approximate calibration.

Particles larger than 0.5 μm are sampled at near atmospheric pressure using the first four stages of the impactor. The last four stages operate at pressures from 150 mm down to 8 mm Hg (absolute) to size segregate the smaller particles. Material deposited at each stage can be analyzed for sulfur containing compounds at the nanogram level by flash volatilization followed by flame photometric analysis (Roberts and Friedlander, 1976). Enough material for chemical analysis can be collected by sampling ambient air with sulfate levels of 10 $\mu g/m^3$ for 15 minutes. The instrument has been checked with ammonium sulfate and sulfuric acid aerosols by comparison with an electrical mobility analyzer. Good agreement between the two instruments was found indicating that the evaporation of these compounds in the impactor was not important. A further check was carried out by sampling simultaneously, in parallel an ammonium sulfate aerosol, with the impactor and a filter. Excellent agreement was obtained.

Measurements have been made of the sulfur mass distribution with respect to particle size with the low pressure impactor. In the absence of strong photochemical conditions, the sulfur mass distribution usually peaks in the size range around 0.5 μm (Figure 6). This is the size range which corresponds to the wave length of the visible light and which is strongly light scattering. The sulfur mass distribution has also been measured with the low pressure impactor during chamber experiments; small quantities of SO_2, propylene and NO-NO_2 were added to unfiltered ambient air exposed to solar radiation. The sulfur mass distribution peaked in the range between 0.1 and 0.2 μm, (Figure 7), significantly smaller than the peak range for the ambient aerosol. (Significant quantities of sulfur in the 0.1 to 0.2 μm range were also measured in one measurement made on a day of strong photochemical activity.)

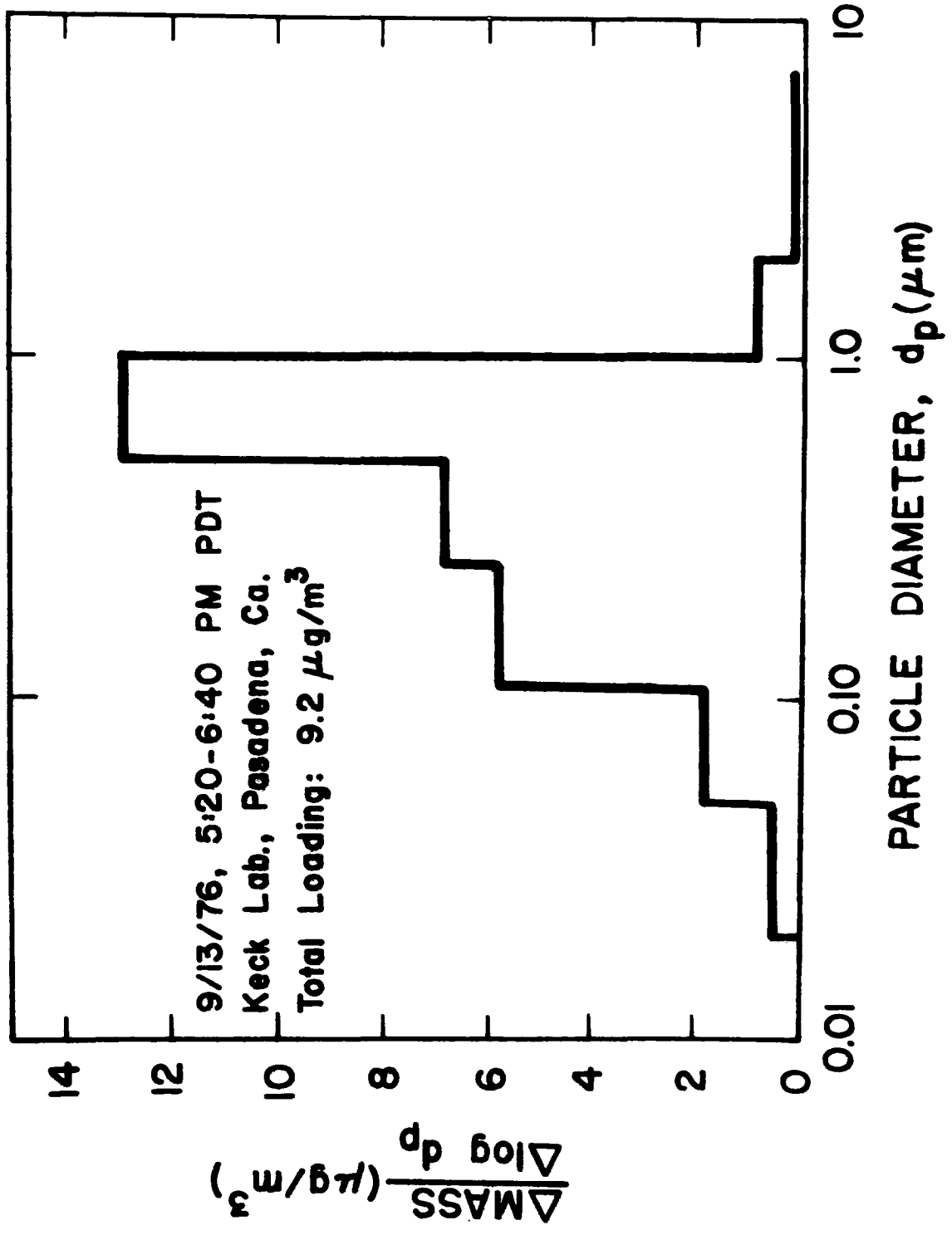

Figure 6. Distribution of sulfur with respect to particle size for the ambient aerosol in Pasadena, California, measured with a low pressure impactor. The peak occurs in the particle size range between 0.5 and 1 μm (Hering, Flagan and Friedlander, 1977).

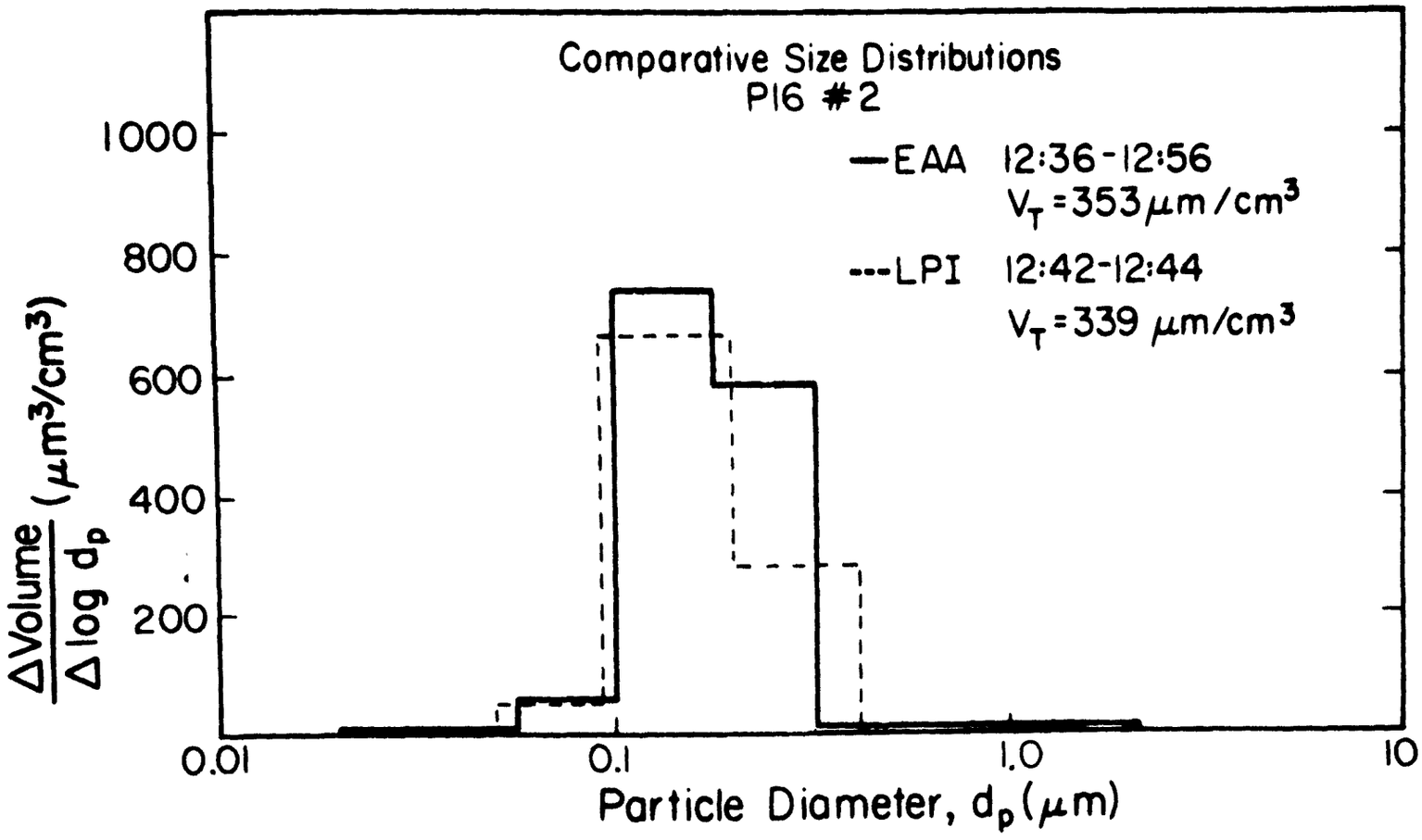

Figure 7. The distribution of sulfur with respect to particle size for a balloon chamber aerosol, measured with the low pressure impactor. SO_2 propylene and NO-NO_2 were added to unfiltered ambient air and the mixture irradiated. A peak in the sulfur distribution developed in the particle size range between 0.1 and 0.2 μm (Hering, Flagan and Friedlander, 1977).

AEROSOL GROWTH DYNAMICS

We consider the case of an aerosol uniformly distributed in a large chamber with particles growing as a result of gas-to-particle conversion. Coagulation and deposition on the walls of the chamber are neglected. This analysis holds best for particles larger than about 0.1 μm in diameter, since particle concentrations in this size range are relatively low and coagulation rates are small.

It is convenient to introduce the continuous size distribution function $n_1(d_p,t)$ defined by the relation

$$dN = n_1(d_p,t)d(d_p) \tag{22}$$

where dN represents the concentration of particles in the size range between d_p and $d_p+d(d_p)$ at time t. The change in $n_1(d_p,t)$ with time in the chamber is given by the expression

$$\frac{\partial n_1}{\partial t} + \frac{\partial n_1 \frac{d(d_p)}{dt}}{\partial d_p} = 0 \tag{23}$$

The distribution of the total aerosol volume with respect to particle diameter is related to the particle size distribution by the expression

$$\frac{\partial V}{\partial \log d_p} = 6 = \frac{\pi}{6} \ln 10\, d_p^4 n_1 \tag{24}$$

The area under the curve of y plotted as a function of $\log d_p$ is proportional to the total particle volume. As a result of gas-to-particle conversion, the total aerosol volume increases with time. Each point on a curve of w vs $\log d_p$ shifts to a new value determined by the growth law. The rate at which any point on the volume distribution function changes with time is given by

$$\frac{dy}{dt} = \frac{\partial y}{\partial t} + w \frac{\partial y}{\partial d_p} \tag{25}$$

where the particle growth rate, w, depends on the mechanism of gas-to-particle conversion (Table 5). By evaluating the right-hand-side of this expression, it is possible to determine the particle size at which the value of w grows most rapidly.

Substitution of (24) in (25) gives

$$\frac{dy}{dt} = \frac{\pi}{5} \ln 10 \left[d_p^4 \left(\frac{\partial n_1}{\partial t} + w \frac{\partial n_1}{\partial d_p} \right) + 4\, w\, n_1 d_p^3 \right] \tag{26}$$

If the particles are much smaller than the mean free path of the gas, and they grow by collision with monomer their volumetric growth rate is proportional to their surface area. The rate of increase in particle diameter with time is constant in this case:

$$w = \frac{d(d_p)}{dt} = \text{constant} \tag{27}$$

When w is constant, substitution in (23) gives:

$$\frac{\partial n_1}{\partial t} + w \frac{\partial n_1}{\partial d_p} = 0 \tag{28}$$

Substitution in (26) the result is

$$\frac{dy}{dt} = \frac{2\pi}{3} \ln 10 \; w \; d_p^3 \; n_1 \tag{29}$$

But the distribution of aerosol surface area with respect to particle size is given by

$$\frac{\partial A}{\partial \log d_p} = \pi \ln 10 \; d_p^3 \; n_1 \tag{30}$$

So

$$\frac{dy}{dt} = \frac{2w\partial A}{3\partial \log d_p} \tag{31}$$

Thus the volume distribution tends to grow most rapidly at the particle size corresponding to a peak in the area distribution function $\frac{\partial A}{\partial \log d_p}$. This is observed, approximately, in chamber experiments with SO_2, propylene and NO-NO_2 in air containing ambient aerosol particles (Figure 7).

DEVIATION BETWEEN THEORY AND EXPERIMENT: SULFATES

Why then does the sulfur mass distribution of the ambient aerosol usually peak at a particle size much larger than the diameter corresponding to the peak in the area distribution function? Although we do not know the answer to this question, there are several possible explanations: 1) The data of Whitby, Husar and Liu (1972) indicate that coagulation can play a significant role in reducing the number concentration of the Los Angeles aerosol between 2000 and 0400 hours (data of September 3, 1969). Over this time period the concentration dropped by a factor of almost 10 while the volume concentration of the aerosol remained almost constant. Thus the mean particle volume increased by a factor of about 2.15 over that time period. Part of this material remains in the air shed and contributes to the sulfate present in the larger particle sizes. The measurements were made at a fixed point in Pasadena so the effect of advection was not taken into account.

2) Certain condensable organic compounds generated by gas phase reactions accumulate preferentially in the particle size range around 0.5 μm. This was the case with two cyclic olefins, cyclopentene and cyclohexene, and one diolefin, 1,7 octadiene, which served as aerosol precursors in experiments reported by Heisler and Friedlander (1977). The experiments were carried out in a baloon reactor; the hydrocarbons and oxides of nitrogen were added to unfiltered ambient air in the chamber and exposed to solar radiation. Difunctional organic compounds produced in this way condense on existing aerosol particles. The rates of particle growth could be correlated by a mechanism based on diffusion to the particles of the condensable gases with a critical particle size near 0.2 μm below which growth did not occur (Kelvin effect). This leads to the development of a peak in the volume distribution in the particle size range, $d_p > 0.5$ m (Heisler and Friedlander, 1977). The area distribution would develop in a size range between 0.2 and 0.5 μm.

Simultaneous experiments with SO_2 were not conducted. If, however, sulfuric acid were formed in such a mixture by the oxidation of SO_2, the H_2SO_4 monomer and small clusters might then be scavenged by the developing peak in the area distribution at a larger particle size than observed in chamber experiments without organic aerosols.

3) If the oxidation of SO_2 takes place in a droplet phase such as a morning fog, the droplet growth rate $\frac{d(d)_p}{dt} \alpha d_p$ (Friedlander, 1977). In this case it can be shown by modifying the analysis of the previous section that the sulfur peak would tend to develop in the size range corresponding to the peak in the volume distribution of the fog. When the fog partially evaporates, the sulfate would be found in a larger particle size range.

DISTRIBUTION OF NITRATE WITH RESPECT TO PARTICLE SIZE (Moskowitz, 1977)

Measurements of aerosol nitrate were made at three locations in the South Coast air basin; Pasadena, Hermosa Beach (30 miles SW of Pasadena, and Chino (an agricultural area 30 miles SE of Pasadena) with the 8 stage, low pressure impactor. Six samples were obtained over the period 7 AM to 7 PM with each sample 1-2 hours in duration. The impactor stages were analyzed using a chemiluminescent NO_x analyzer the same day.

The data for the three locations for each run are shown in Figure 8. It is seen that in midmorning, regardless of location, there is a significant quantity of particulate matter in the submicron range. This is also apparent in the late afternoon data of Chino and Pasadena.

An average diurnal nitrate size distribution for each location was obtained by time averaging the nitrate levels present on like stages of the impactor. The Pasadena distribution was bimodal with peaks in the two size ranges 0.05-1 μm and 2-8 μm (8 μm is an arbitrary upper cutoff). The Chino data, near an ammonia rich cattle feed area, showed a peak in the submicron range although the distribution was weakly bimodal. In the coastal area the predominant size range for nitrates was in the 2-8 μm region. Pasadena may be throught of as possessing aerosol characteristics of both coastal and agricultural regions.

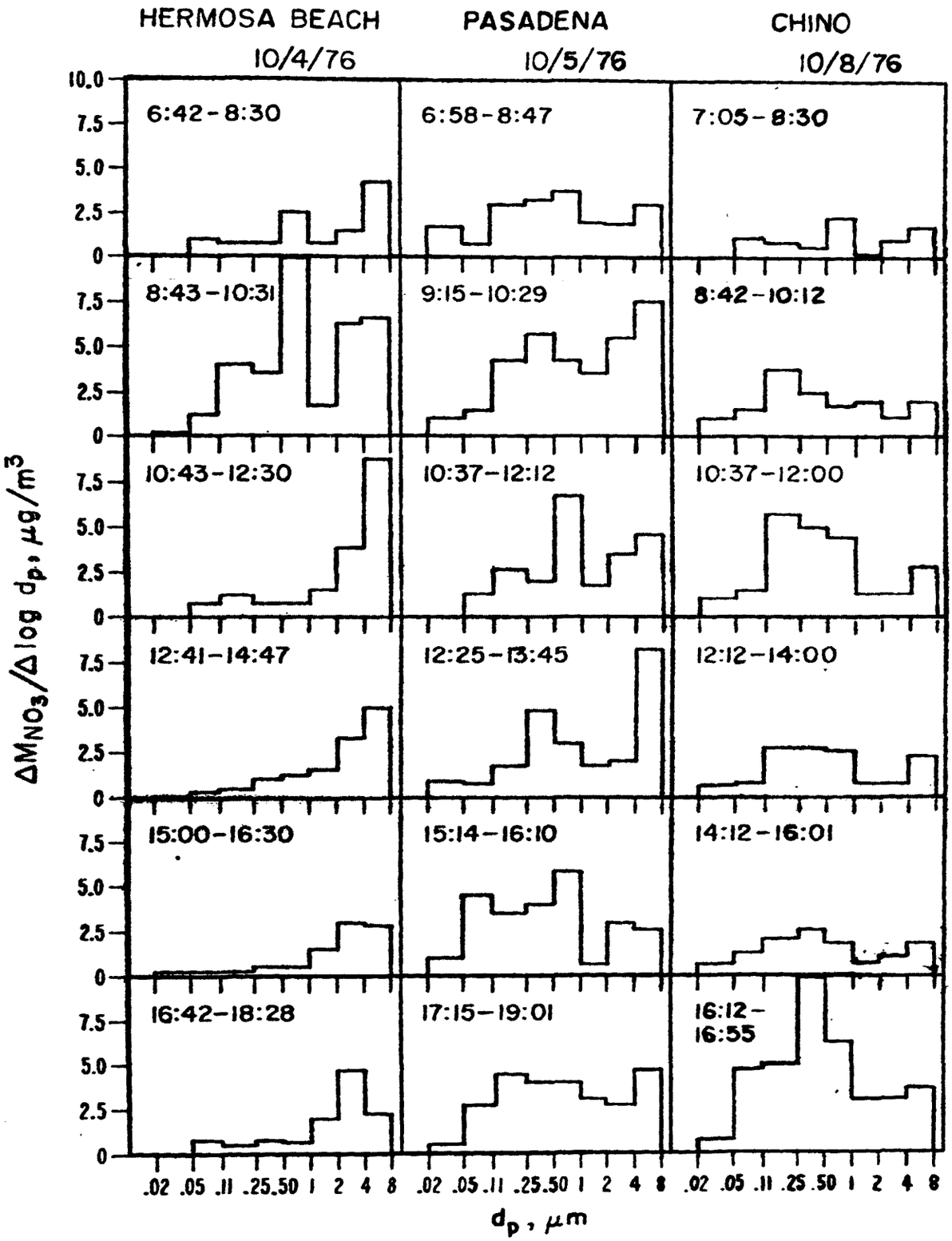

Figure 8. Aerosol nitrate distributions with respect to particle size for different locations at various times of day.

In an investigation by O'Brien et al. (1975), inorganic nitrate and other particulate pollutants were measured in a number of California locations. It was found that inorganic nitrate (NH_4NO_3 and $NaNO_3$) of a secondary or photochemical origin contributed about 10% of the mass loading in the South Coast air basin. The prevalent form of nitrate in the basin was NH_4NO_3; the NH_4^+ concentration was the highest in the Los Angeles air basin compared to other California locations. The study also showed that the coastal Santa Barbara sample contained 16% inorganic nitrate while the NH_4^+ concentration was essentially zero. This indicates that the reaction of NO_2 with NaCl is of importance in coastal areas:

$$3NO_2 + H_2O = 2HNO_3 + NO$$

$$HNO_3 + NaCl = NaNO_3 + HCl$$

The data indicate that the Pasadena aerosol consists of both small NH_4NO_3 and larger $NaNO_3$ particles.

Nitrogen (as nitrate) gas-particle distribution factors were calculated for the Pasadena data. The distribution factor f_N is defined as:

$$f_N = \frac{NO_3^-}{NO_x + NO_3^-}$$

where NO_3^- = particulate nitrate concentration, as NO_2, $\mu g/m^3$ and NO_x = gas phase concentration as NO_2, converted from ppm to $\mu g/m^3$, averaged over the sampling period. The distribution factors ranged from 2.5 to 22.8% in the same range reported by Grosjean and Friedlander (1975).

It is of interest to look at the amounts of $NaNO_3$ which would correspond to the ambient levels of Na. Sodium was measured in the ACHEX experiment (Hidy, et al. 1975) and the concentration was about 0.7 $\mu g/m^3$. This corresponds to a level of 1.89 $\mu g/m^3$ of NO_3^-. If one time averages the levels of particles with diameter greater than 2.0 μm for each of the locations it is found that beach nitrate is 2.6 $\mu g/m^3$, Pasadena 2.5 $\mu g/m^3$, and Chino 1.0 $\mu g/m^3$. This would be consistent with the hypothesis that the concentration of Na should decrease as one moves inland, with decreasing levels of large particles. The concentration of large particles in Pasadena is consistent with the concentration predicted by ambient Na levels.

The results of the ACHEX study indicated that on a mass basis, the nitrate component of the aerosol contributed less to light scattering than the sulfate. The explanation for this effect may be that most of the sulfate exists in a highly efficient light scattering range (0.1-1.0 μm) whereas only part of the nitrate is found in this range.

REFERENCES

1. Calvert, J. G. (1973) "Interactions of Air Pollutants" in Proceedings of the Conference on Health Effects of Air pollutants, U. S. Govt. Printing Office Serial No. 93-15.

2. Frenkel, J. (1955) Kinetic Theory of Liquids, Dover.

3. Friedlander, S. K. (1977) Smoke, Dust and Haze: Fundamentals of Aerosol Behavior, Wiley-Interscience, New York.

4. Friedlander, S.K. (1978) Atmos. Environ., 12, 187.

5. Fuchs, N. A. and Sutugin, A. G. (1971) "Highly-Dispersed Aerosols" in Hidy, G. M. and Brock, J. R. (Eds.) Topics in Current Aerosol Research, Pergamon Press.

6. Grosjean, D. and Friedlander, S. K. (1975) JAPCA 25, 1038.

7. Grosjean, D. and Friedlander, S. K. (1978) "Formation of Organic Aerosols from Cyclic Olefins and Diolefins" based on work done on EPA Grant No. R 802160. Submitted for publication.

8. Heisler, S. L. and Friedlander, S. K. *1977) Atmos. Environ., 11, 185.

9. Heist, R. H. and Reiss, H. (1971) J. Chem. Phys. 59, 665.

10. Hering, S. V., Flagan, R. C. and Friedlander, S. K. (1978) Environ. Sci. Technol. 12, 667.

11. Hidy, G. M. (Ed.) (1975) "Characterization of Aerosols in California" (ACHEX). Final Report to Air Resources Board, State of California, ARB Contract No. 358.

12. Hidy, G. M. and Friedlander, S. K. (1971) "The Nature of the Los Angeles Aerosol" in Proceedings, 2nd Intl. Clean Air Congress, Englund, H. M. & Berry, W. T. (Eds.) Academic Press, New York.

13. Katz, J. L., Scoppa, C. J., Kumar, N. G. and Mirabel, P. (1975), J. Chem. Phys. 62, 448.

14. Kiang, C. S. and Stauffer, D. (1973) Faraday Symposia of the Chemical Society, No. 7, 29.

15. Mason, B. J. (1971) The Physics of Clouds, Clarendon Press, Oxford.

16. McMurry, P. H., On the Relationship Between Aerosol Dynamics and the Rate of Gas-to-Particle Conversion. Ph.D. Dissertation in Environmental Engineering Science, California Institute of Technology, (1977).

17. Moskowitz, A. H. "Particle Size Distribution of Nitrate Aerosols in the Los Angeles Air Basin," EPA-600/3-77-053, May 1977.

18. O'Brien, R. J., Crabtree, J. H., Holmes, J. R., Huggan, M. C. and Bockian, A. H. (1975) Environ. Sci. and Technol. 9, 577.

19. Reiss, H. (1950) J. Chem. Phys. 18, 840.

20. Roberts, P. T. and Friedlander, S. K. (1975) Environmental Health Perspectives 10, 103.

21. Roberts, P. T. and Friedlander, S. K. (1976) Environ. Sci. Technol. 10, 573.

22. Sander, S. P. and Seinfeld, J. H. (1976) Environ. Sci. Technol. 10, 1114.

23. Whitby, K. T., Husar, R. B. and Liu, B. Y. H. (1972), J. Colloid Interface Sci. 39, 177.

APPENDIX A

PROJECT DISSERTATIONS AND PUBLISHED PAPERS

THESES

Ph.D.

Roberts, P. T. "Gas-to-Particle Conversion: Sulfur Dioxide in a Photochemically Reactive System" (1975)

Heisler, S. L. "Gas-to-Particle Conversion in Photochemical Smog: Growth Laws and Mechanisms for Organics" (1975)

McMurry, P. H. "On the Relationship Between Aerosol Dynamics on the Rate of Gas-to-Particle Conversion" (1977)

MS

Moskowitz, A. "The Distribution of Aerosol Nitrate Compounds with Respect to Particle Size: Vaporization Analysis with the Low Pressure Impactor" (1977)

PUBLICATIONS

Friedlander, S. K. (1978) Atmos. Environ., 12, 187.

Grosjean, D. and Friedlander, S. K. (1975) JAPCA 25, 1038.

Grosjean, D. and Friedlander, S. K. (1978) "Formation of Organic Aerosols from Cyclic Olefins and Diolefins" based on work done on EPA Grant No. R802160. Submitted for publication.

Heisler, S. L. and Friedlander, S. K. (1977) Atmos. Environ. 215.

Hering, S. V., Flagan, R. C. and Friedlander, S. K. (1978) Environ. Sci. Technol. 12, 667.

Moskowitz, A. H, "Particle Size Distribution of Nitrate Aerosols in the Los Angeles Air Basin," EPA-600/3-77-053, May 1977.

Roberts, P. T. and Friedlander, S. K. (1975) Environmental Health Perspectives 10, 103.

Roberts, P. T. and Friedlander, S. K. (1976) Environ. Sci. Technol. 10, 573.

TECHNICAL REPORT DATA
(Please read Instructions on the reverse before completing)

1. REPORT NO. EPA-600/3-79-052	2.	3. RECIPIENT'S ACCESSION NO.
4. TITLE AND SUBTITLE PHOTOCHEMICAL AEROSOL DYNAMICS		5. REPORT DATE May 1979
		6. PERFORMING ORGANIZATION CODE
7. AUTHOR(S) S.K. Friedlander		8. PERFORMING ORGANIZATION REPORT NO.
9. PERFORMING ORGANIZATION NAME AND ADDRESS Department of Chemical Engineering, California Institute of Technology, Pasadena, CA 91125		10. PROGRAM ELEMENT NO. 1AA603A AC-16 (FY-78)
		11. CONTRACT/GRANT NO. R802160
12. SPONSORING AGENCY NAME AND ADDRESS Environmental Sciences Research Laboratory - RTP, NC; Office of Research and Development; U.S. Environmental Protection Agency; Research Triangle Park, North Carolina 27711		13. TYPE OF REPORT AND PERIOD COVERED Final 4/73-3/78
		14. SPONSORING AGENCY CODE EPA/600/09

15. SUPPLEMENTARY NOTES

16. ABSTRACT

New data are reported on (1) the rate of formation of condensable chemical species by photochemical reactions, (2) the effect of the reaction products on the particle size distribution and (3) the distribution of reaction products as a function of particle size. Gas-to-particle conversion for cyclopentene, cyclohexene and 1,7-octadiene, ranged from 5 to 39 percent of the initial gas-phase carbon concentrations. Size distribution data for cyclohexene were correlated by a diffusion controlled growth law with a Kelvin cutoff diameter at about 0.25 μm.

In polluted atmospheres, some new particle formation takes place as a result of homogeneous gas phase reactions even though an aerosol is already present. To explain the results of laboratory studies of this phenomenon, classical nucleation theory must be modified to take into account the scavenging of clusters by the aerosol. Using a new low pressure impactor, the first measurements have been made of the distributions of sulfate and nitrate with respect to particle size for $d_p < 0.25$ μm. In Pasadena, the data for sulfate often show a peak in the mass distribution for $0.6 < d_p < 1.0$ μm; less often, a peak is observed near 0.1 μm, consistent with laboratory data for aerosols formed by homogeneous gas phase reactions.

17. KEY WORDS AND DOCUMENT ANALYSIS

a. DESCRIPTORS	b. IDENTIFIERS/OPEN ENDED TERMS	c. COSATI Field/Group
Air pollution *Aerosols *Photochemical reactions *Particle size distribution		13B 07D 07E

18. DISTRIBUTION STATEMENT RELEASE TO PUBLIC	19. SECURITY CLASS (This Report) UNCLASSIFIED	21. NO. OF PAGES 46
	20. SECURITY CLASS (This page) UNCLASSIFIED	22. PRICE

EPA Form 2220-1 (9-73)